Matrix lattice Boltzmann reloaded

By Ilya Karlin[1,2], Pietro Asinari[3], Sauro Succi[4,5]

[1] Aerothermochemistry and Combustion Systems Lab, ETH Zurich, 8092 Zurich, Switzerland

[2] School of Engineering Sciences, University of Southampton, SO17 1BJ Southampton, UK

[3] Department of Energetics, Politecnico di Torino, 10129 Torino, Italy

[4] Istituto Applicazioni Calcolo CNR, Via dei Taurini 19, 00185 Roma, Italy

[5] Freiburg Institute for Advanced Studies, School of Soft Matter Research, Albert-Ludwigs-Universitt Freiburg, Albertstr. 19, 79104 Freiburg, Germany

The lattice Boltzmann equation has been introduced about twenty years ago as a new paradigm for computational fluid dynamics. In this paper, we revisit the main formulation of the lattice Boltzmann collision integral (matrix model) and introduce a new two-parametric family of collision operators which permits to combine enhanced stability and accuracy of matrix models with the outstanding simplicity of the most popular single-relaxation time schemes. The option of the revised lattice Boltzmann equation is demonstrated through numerical simulations of a three-dimensional lid driven cavity.

Keywords: Lattice Boltzmann

1. Introduction

Twenty years ago, the first computationally competitive lattice Boltzmann scheme was introduced in a form whereby inter-particle collisions are represented through a scattering matrix between the various discrete-velocity Boltzmann distributions living on the same node of the spatial lattice (Higuera et al., 1989). By prescribing the spectral structure of the scattering matrix based on the desired macroscopic target equations (Navier-Stokes) rather than on an underlying microscopic dynamics, this top-down formulation permitted to achieve values of the Reynolds number as high as allowed by the grid resolution, whence making the first competitive contact with computational fluid dynamics at large (see, e. g. the earliest review (Benzi et al., 1992), as a well as the most recent review (Aidun and Clausen, 2010) covering lattice Boltzmann applications in many fields of fluid dynamics, from turbulence to micro-flows, and references therein). The original matrix formulation was quickly superseded by the so-called lattice Bhatnagar-Gross-Krook (LBGK) equation, in which the scattering matrix is reduced to a diagonal form, with a single parameter controlling the relaxation rate of fluid momentum (viscosity), as well as any other non-conserved kinetic moment (Chen et al., 1992; Qian et al., 1992). Despite its obvious limitations, namely all kinetic modes relaxing at the same pace to local equilibrium, the LBGK has rapidly taken a dominant role in the field, mostly on account of its simplicity. Around the same time as LBGK, the original matrix version has been revisited, optimized and turned in what has now come to be known as multiple relaxation time (MRT) lattice Boltzmann (d'Humières, 1992; d'Humières

et al., 2002; Shan and Chen, 2007), recently with improved Galilean invariance by the so-called cascaded formulation (Geier et al., 2006). Although the MRT provides a useful outgrowth of LBGK, the mainstream of lattice Boltzmann research remains with LBGK, due to its unsurpassed simplicity.

Under such state of affairs, it appears that an optimum compromise between the enhanced stability and flexibility of MTR and the computational handiness of LBGK is much needed. In this work, we shall present precisely such type of optimum compromise. We introduce a new scheme (revised matrix LB equation, RM hereafter) which aims at combining the best of the two options, namely enhanced stability with virtually the same simplicity as LBGK. Our option is based on a *two-step* relaxation BGK-like collision operator, in which the two time-scales describe relaxation to two *distinct* equilibria, one of which is the (usual) fixed point of the relaxation and the other is an intermediate (quasi-equilibrium) state. Models of this type are well known in kinetic theory (see, e. g. (Gorban and Karlin, 1994) and references therein) and are used to achieve a description of fluids with realistic Prandtl or Schmidt numbers not possible with BGK. At variance with previous formulations, the present RM method is aimed at boosting the stability and accuracy of athermal lattice Boltzmann models in the incompressible limit. In this paper, we provide an example of the RM construction on the commonly used 19-velocity lattice which retains much of the factorization property. On the practical side, the RM numerical algorithm is pretty simple: all it takes is just a few lines changes in existing LBGK codes. Supporting numerical evidence is provided through the simulation of a lid driven cavity which shows viability of the revised matrix model.

2. Lattice Boltzmann method

(a) Matrix LB model

Let us denote $f(\boldsymbol{x}, t)$ a vector of populations f_i corresponding to the D-dimensional discrete velocities $\boldsymbol{v}_i$, $i = 1, \dots, b$, at the site $\boldsymbol{x}$ at time t. Throughout the paper, we denote $\langle \dots \rangle$ a sum over the discrete velocity index. The matrix lattice Boltzmann equation for the incompressible flow simulation has the form (Higuera et al., 1989)

$$f(\boldsymbol{x} + \boldsymbol{v}, t + 1) - f(\boldsymbol{x}, t) = A(f - f^{\mathrm{eq}}), \qquad (2.1)$$

where f^{eq} is a local equilibrium which depends on $\rho = \langle f \rangle$ (local density) and $\rho \boldsymbol{u} = \langle \boldsymbol{v} f \rangle$ (local momentum with $\boldsymbol{u}$ the local flow velocity). The spectral properties and computer implementation of the scattering matrix A are extensively discussed in (d'Humières, 1992; d'Humières et al., 2002). If $A = -\omega_1 \mathrm{Id}$, where Id is the identity matrix, then the matrix lattice Boltzmann (2.1) reduces to a one-parametric lattice Bhatnagar-Gross-Krook (LBGK) model (Chen et al., 1992; Qian et al., 1992),

$$f(\boldsymbol{x} + \boldsymbol{v}, t + 1) - f(\boldsymbol{x}, t) = -\omega_1 (f - f^{\mathrm{eq}}). \qquad (2.2)$$

With the equilibrium f^{eq} satisfying the isotropy conditions for the pressure tensor $\rho \Pi_{\alpha\beta} = \langle v_\alpha v_\beta f \rangle$ and the third-order moment $Q_{\alpha\beta\gamma} = \langle v_\alpha v_\beta v_\gamma f \rangle$,

$$\rho \Pi_{\alpha\beta}^{\mathrm{eq}} = \rho c_{\mathrm{s}}^2 \delta_{\alpha\beta} + \rho u_\alpha u_\beta, \qquad (2.3)$$

$$\rho Q_{\alpha\beta\gamma}^{\mathrm{eq}} = \rho c_{\mathrm{s}}^2 (u_\alpha \delta_{\beta\gamma} + u_\beta \delta_{\alpha\gamma} + u_\gamma \delta_{\alpha\beta}) + O(u^3), \qquad (2.4)$$

where c_{s} is the lattice speed of sound, the LBGK model (2.2) remains the most popular to date version of LB for the simulation of incompressible flow, mostly due to its outstanding simplicity.

(b) Matrix LB reloaded model

A characteristic property of the matrix LB equation (2.1) is that only one state is specified (the local equilibrium f^{eq}). We here suggest a different two-parametric family of LB equations based on an intermediate (quasi-equilibrium) state of relaxation f^{C},

$$f(\boldsymbol{x} + \boldsymbol{v}, t + 1) - f(\boldsymbol{x}, t) = -\omega_1(f - f^{\text{C}}) - \omega_2(f^{\text{C}} - f^{\text{eq}}). \tag{2.5}$$

Let us introduce a local temperature variable Θ (D is space dimension),

$$\rho\Theta = D^{-1} \left\langle (\boldsymbol{v} - \boldsymbol{u})^2 f \right\rangle. \tag{2.6}$$

With this, we consider an intermediate state f^{C} which satisfies the following properties:

$$\left\langle f^{\text{C}} \right\rangle = \rho, \ \left\langle \boldsymbol{v} f^{\text{C}} \right\rangle = \rho\boldsymbol{u}, \tag{2.7}$$

$$f^{\text{C}}(f^{\text{eq}}) = f^{\text{eq}}, \tag{2.8}$$

$$\left\langle v_\alpha v_\beta f^{\text{C}} \right\rangle = \rho\Lambda(\Theta)\delta_{\alpha\beta} + \rho u_\alpha u_\beta, \ \Lambda(c_{\text{s}}^2) = c_{\text{s}}^2, \ d\Lambda/d\Theta\big|_{\Theta = c_{\text{s}}^2} = \lambda \geq 0. \tag{2.9}$$

Condition (2.7) maintains the local density and momentum conservation, while condition (2.8) guarantees the zero of collision integral is at the local equilibrium. Finally, condition (2.9) regulates the pressure tensor $\rho\Pi_{\alpha\beta}^{\text{C}}$ at the intermediate state of relaxation. Two limiting cases are most interesting: at $\lambda = 0$, this tensor is kept at the equilibrium, $\Pi_{\alpha\beta}^{\text{C}} = \Pi_{\alpha\beta}^{\text{eq}}$, while the choice $\Lambda = \theta$ ($\lambda = 1$) corresponds to the familiar ideal gas equation of state. When the two relaxation parameters are equal ($\omega_1 = \omega_2$), Eq. (2.5) reduces to the LBGK (2.2). On the other hand, Eq. (2.5) can be written in the LBGK-like form:

$$f(\boldsymbol{x} + \boldsymbol{v}, t + 1) - f(\boldsymbol{x}, t) = -\omega_1(f - f^{\text{GE}}), \tag{2.10}$$

where a generalized equilibrium f^{GE},

$$f^{\text{GE}} = \frac{\omega_2}{\omega_1} f^{\text{eq}} + \left(1 - \frac{\omega_2}{\omega_1}\right) f^{\text{C}}. \tag{2.11}$$

is a convex (due to realizability condition, $\omega_2/\omega_1 \leq 1$) combination between f^{C} and f^{eq}. As we shall see it below, the proper choice of f^{C} endows the LBGK-like relaxation process (2.10) with some valuable properties not accessible to the single-time LBGK scheme (2.2).

With an intermediate state f^{C} satisfying the conditions (2.7), (2.8) and (2.9) the two-parametric family of *revised matrix* (RM) equations (2.5) recovers the athermal Navier-Stokes equations with the kinematic (shear) viscosity ν and the second (bulk) viscosity ξ as follows

$$\nu = \left(\frac{1}{\omega_1} - \frac{1}{2}\right) c_{\text{s}}^2, \tag{2.12}$$

$$\xi = \left(\frac{1}{\lambda(\omega_2 - \omega_1) + \omega_1} - \frac{1}{2}\right) c_{\text{s}}^2. \tag{2.13}$$

Shear viscosity ν (2.12) is the only transport coefficient which remains pertinent in the low-Mach number (incompressible flow) limit. In that respect, the two-parametric RM family defines an equivalence class of LB models for the incompressible flow simulation, with the LBGK being a particular element of this family. On the contrary, the second (bulk) viscosity coefficient depends on the choice of f^{C}. Note that, as it is pertinent to the kinetics without the energy conservation, the slope of the pressure $\rho\Lambda$ with respect to the "temperature" Θ in (2.9) defines the ratio between the bulk and the shear viscosity. In the two limiting cases mentioned above, we have: at $\lambda = 0$, the shear and bulk viscosities are equal, while at $\lambda = 1$, the bulk viscosity is decoupled from the shear, and is defined by the second relaxation parameter ω_2 alone (and thus ξ can be regarded a free tunable parameter to enhance numerical stability (Asinari and Karlin, 2009; Dellar, 2001)). In certain cases when the intermediate state f^{C} can be described as the minimum of the entropy function, one can prove that the bulk viscosity in the present model should be larger or equal to the shear (see, e. g. (Asinari and Karlin, 2009)). Note that conditions (2.7), (2.8) and (2.9) do not yet define the intermediate state f^{C} uniquely, and the actual performance of the scheme may be strongly effected by a particular choice of f^{C}. For example, even for $\lambda = 0$, the RM is not necessary equivalent to the LBGK, even though they share the same shear and bulk viscosities.

(c) *Unidirectional quasi-equilibrium on the Maxwell lattice*

The essential ingredient of the RM model (2.5) is the intermediate state of relaxation f^{C}, which needs to be explicitly designed so as to accomplish the aforementioned optimization. This task is facilitated by considering a specific family of populations, providing a universal template for constructing various f^{C} with tailored properties (Asinari and Karlin, 2009; Karlin and Asinari, 2010).

In the dimension $D = 2, 3$, the fundamental Maxwell lattices are generated by a tensor product of D copies of the one-dimensional velocities $\{-1, 0, 1\}$ (the D2Q9 and D3Q27 lattices) which we consider first. For $D = 3$, the discrete velocities are denoted as $v = (i, j, k)$, $i, j, k \in \{-1, 0, 1\}$ in a fixed Cartesian coordinate system. A weight $W_{(i,j,k)} = W_{(i)}W_{(j)}W_{(k)}$ corresponds to each velocity where $W_{(0)} = 2/3$ and $W_{(-1)} = W_{(1)} = 1/6$ are one-dimensional weights, while the speed of sound $c_{\mathrm{s}} = 1/\sqrt{3}$ is independent of the dimension. With this, the entropy function of the D3Q27 model is defined as $H = \langle f \ln(f/W) \rangle$ (Karlin et al., 1999).

Following Asinari and Karlin (2009); Karlin and Asinari (2010), for D3Q27, we define a special *unidirectional quasi-equilibrium* population (UniQuE) f^* as a minimizer of the entropy function H under fixed density, momentum, and three diagonal components of the pressure tensor,

$$\rho\Pi_{xx} = \left\langle v_{(i)}^2 f_{(i,j,k)} \right\rangle, \; \rho\Pi_{yy} = \left\langle v_{(j)}^2 f_{(i,j,k)} \right\rangle, \; \rho\Pi_{zz} = \left\langle v_{(k)}^2 f_{(i,j,k)} \right\rangle. \qquad (2.14)$$

Minimization is achieved by a fully factorized UniQuE population,

$$f^*_{(i,j,k)} = \rho\varphi_{(i)}(u_x, \Pi_{xx})\varphi_{(j)}(u_y, \Pi_{yy})\varphi_{(k)}(u_z, \Pi_{zz}), \qquad (2.15)$$

where

$$\varphi_{(l)}(u_\alpha, \Pi_{\alpha\alpha}) = \frac{1}{2^{|l|}} \left[(1 - |l|) + lu_\alpha + (2|l| - 1)\Pi_{\alpha\alpha}\right], \; l \in \{-1, 0, 1\}. \qquad (2.16)$$

We further refer to the three-tuple (2.16) as a *unidirectional particle* (in a direction α). The UniQuE is the main source for derivations of the intermediate states of relaxation f^{C}, with tailored properties for RM.

(*d*) *UniQuE on sub-Maxwell lattices*

The two sub-lattices of the D3Q27 which also satisfy the isotropy relation (2.4) are known as the D3Q19 and D3Q15 lattices. In this case, analog of the UniQuE (2.15) is readily constructed by a projection pruning algorithm (Karlin and Asinari, 2010). Let us introduce a unidirectional *anti*-particle, that is a three-tuple

$$\psi_{(l)}(u_\alpha, \Pi_{\alpha\alpha}) = \frac{1}{2^{|l|}}\left[lu_\alpha + (2|l| - 1)\Pi_{\alpha\alpha}\right], \; l \in \{-1, 0, 1\}. \tag{2.17}$$

The (analog of) UniQuE on D3Q19 is then represented as a difference between the factorized distributions of unidirectional particles and of the antiparticles:

$$\begin{aligned}
f^*_{(i,j,k)} =& \rho\varphi_{(i)}(u_x, \Pi_{xx})\varphi_{(j)}(u_y, \Pi_{yy})\varphi_{(k)}(u_z, \Pi_{zz}) \\
&- \rho\psi_{(i)}(u_x, \Pi_{xx})\psi_{(j)}(u_y, \Pi_{yy})\psi_{(k)}(u_z, \Pi_{zz}).
\end{aligned} \tag{2.18}$$

3. Example of the RM LB model on D3Q19 lattice

Recent studies indicated that kinetic modes, stemming from the dynamics of the third-order moments can severely affect stability of the LBGK (d'Humières et al., 2002; Ginzburg, 2005; Geier et al., 2006). Decoupling of the relaxation of the third-order moments $\rho Q_{\alpha\beta\beta}$ from the relaxation of the rest of the moments represents therefore our objective here in constructing the intermediate state f^{C} for RM. In order to construct the corresponding intermediate state f^{C} from the UniQuE of the D3Q19 lattice (2.18), the following two steps are taken: (i) Unbias the third order UniQuE moments $Q^*_{\alpha\beta\beta} = \rho u_\alpha \Pi_{\beta\beta}$: Replace $u_\alpha\Pi_{\beta\beta} \rightarrow Q_{\alpha\beta\beta}$, in (2.18) where $\rho Q_{\alpha\beta\beta}$ is the corresponding third order moment evaluated at the current population f; (ii) Equilibrate the rest of the moments: Replace $\Pi_{\alpha\alpha} \rightarrow \Pi^{\mathrm{eq}}_{\alpha\alpha} = c_{\mathrm{s}}^2 + u_\alpha^2$. Furthermore, the local equilibrium f^{eq} is constructed by equilibration of all the moments $\Pi_{\alpha\alpha} \rightarrow \Pi^{\mathrm{eq}}_{\alpha\alpha}$ in f^* (2.18). The intermediate state f^{C} and the equilibrium f^{eq} can be combined into the generalized equilibrium f^{GE} (2.11):

$$\begin{aligned}
f^{\mathrm{GE}}_{(0,0,0)} =& \rho[1 - \Pi^{\mathrm{eq}}_{xx} - \Pi^{\mathrm{eq}}_{yy} - \Pi^{\mathrm{eq}}_{zz} + \Pi^{\mathrm{eq}}_{xx}\Pi^{\mathrm{eq}}_{yy} + \Pi^{\mathrm{eq}}_{yy}\Pi^{\mathrm{eq}}_{zz} + \Pi^{\mathrm{eq}}_{xx}\Pi^{\mathrm{eq}}_{zz}], \\
f^{\mathrm{GE}}_{(\sigma,0,0)} =& \frac{\rho}{2}\left[(1 - \Pi^{\mathrm{eq}}_{yy} - \Pi^{\mathrm{eq}}_{zz})\Pi^{\mathrm{eq}}_{xx} + \sigma u_x - \sigma(Q^{\mathrm{GE}}_{xyy} + Q^{\mathrm{GE}}_{xzz})\right], \\
f^{\mathrm{GE}}_{(0,\mu,0)} =& \frac{\rho}{2}\left[(1 - \Pi^{\mathrm{eq}}_{xx} - \Pi^{\mathrm{eq}}_{zz})\Pi^{\mathrm{eq}}_{yy} + \mu u_y - \mu(Q^{\mathrm{GE}}_{yxx} + Q^{\mathrm{GE}}_{yzz})\right], \\
f^{\mathrm{GE}}_{(0,0,\delta)} =& \frac{\rho}{2}\left[(1 - \Pi^{\mathrm{eq}}_{xx} - \Pi^{\mathrm{eq}}_{yy})\Pi^{\mathrm{eq}}_{zz} + \delta u_z - \delta(Q^{\mathrm{GE}}_{zyy} + Q^{\mathrm{GE}}_{zxx})\right], \\
f^{\mathrm{GE}}_{(\sigma,\mu,0)} =& \frac{\rho}{4}(\Pi^{\mathrm{eq}}_{xx}\Pi^{\mathrm{eq}}_{yy} + \sigma\mu u_x u_y + \sigma Q^{\mathrm{GE}}_{xyy} + \mu Q^{\mathrm{GE}}_{yxx}), \\
f^{\mathrm{GE}}_{(0,\mu,\delta)} =& \frac{\rho}{4}(\Pi^{\mathrm{eq}}_{zz}\Pi^{\mathrm{eq}}_{yy} + \delta\mu u_z u_y + \delta Q^{\mathrm{GE}}_{zyy} + \mu Q^{\mathrm{GE}}_{yzz}), \\
f^{\mathrm{GE}}_{(\sigma,0,\delta)} =& \frac{\rho}{4}(\Pi^{\mathrm{eq}}_{zz}\Pi^{\mathrm{eq}}_{xx} + \delta\sigma u_z u_x + \delta Q^{\mathrm{GE}}_{zxx} + \sigma Q^{\mathrm{GE}}_{xzz}),
\end{aligned} \tag{3.1}$$

where $\sigma, \mu, \delta \in \{-1, 1\}$, and

$$Q_{\alpha\beta\beta}^{\mathrm{GE}} = \left(1 - \frac{\omega_2}{\omega_1}\right) Q_{\alpha\beta\beta} + \frac{\omega_2}{\omega_1} u_\alpha (c_{\mathrm{s}}^2 + u_\beta^2), \ \Pi_{\alpha\alpha}^{\mathrm{eq}} = c_{\mathrm{s}}^2 + u_\alpha^2, \ c_{\mathrm{s}}^2 = \frac{1}{3}. \quad (3.2)$$

Substituting the generalized equilibrium (3.1), (3.2) into the LBGK-like form (2.10), we set up the RM model on the D3Q19 lattice. Finally, in order to spell out the various distributions used in the combined generalized equilibrium (3.1), we note that the equilibrium (fixed point of the collisions) is obtained upon setting $\omega_1 = \omega_2$ in (3.2), while the intermediate state corresponds to $\omega_2 = 0$.

We shall now proceed with a numerical validation of the present scheme. For that, we have chosen the diagonally lid-driven 3D cavity flow, the standard test for LB models suggested in (d'Humières et al., 2002). The cavity is a cubic box with an unit edge and it fits into a Cartesian coordinate system, namely (x, y, z). The boundary condition at the top plane $(x, y, 1)$ is $\boldsymbol{u}_L = (\sqrt{2}, \sqrt{2}, 0)/20$ so that $u_L = \|\boldsymbol{u}_L\| = 1/10$. The other five planes are subject to no-slip boundary conditions. The kinematic (shear) viscosity is equal to $\nu = 3/1000$. The computational domain is discretized by a uniform collocated grid with N^3 points with $N = 60$. The boundaries are located half-cell away from the computational nodes. Hence the Reynolds number is Re = 2000 and consequently the relaxation parameter controlling the kinematic viscosity is equal to $\omega_1 = 1000/509 \approx 1.9646$. Let us denote $\boldsymbol{x}_w$ the generic boundary computational node. In all inner computational nodes $(\boldsymbol{x} \neq \boldsymbol{x}_w)$, Eq. (2.5) holds for any lattice velocity $\boldsymbol{v}_i$. Following (d'Humières et al., 2002), in the generic boundary computational node $\boldsymbol{x}_w$, the following condition holds $f(\boldsymbol{x}_w, t + \delta t) = f^{\mathrm{eq}}(\rho_w, \boldsymbol{u}_w)$, where $\rho_w = (1 - \eta_w)\rho(\boldsymbol{x}_w + \boldsymbol{n}_w, t) + \eta_w \, \rho(\boldsymbol{x}_w, 0)$, $\boldsymbol{u}_w = \boldsymbol{u}_d + \frac{1}{3}\left(\boldsymbol{u}(\boldsymbol{x}_w + \boldsymbol{n}_w, t) - \boldsymbol{u}_d\right)$, where η_w is a tunable parameter, $\boldsymbol{n}_w$ is the vector normal to the wall and pointing towards the fluid (e.g. $\boldsymbol{n}_w = (0, 0, -1)$ for the sliding wall) and $\boldsymbol{u}_d$ is the desired velocity at the wall (located half-cell away from the computational node). In particular, $\eta_w = 0$ and $\boldsymbol{u}_d = \boldsymbol{0}$ for all the walls, with the exception of the sliding wall for which $\eta_w = 1$ and $\boldsymbol{u}_d = \boldsymbol{u}_L = (\sqrt{2}, \sqrt{2}, 0)/20$. Finally, the number of time steps (roughly $18,000$) has been selected in order to reach $E(t+1)/E(t) - 1 \leq 5 \times 10^{-5}$, where $E(t)$ is the total kinetic energy in the cavity. In summary, the boundary conditions and the Reynolds number are taken from the MRT setup studied in (d'Humières et al., 2002) in order to make a comparison of the performance of various lattice Boltzmann models.

Three different models are considered for the bulk equation, namely (i) LBGK model: Eq. (2.1) with $A = -\omega_1 \mathrm{Id}$; (ii) MRT model: Eq. (2.1) with the scattering matrix A as given in Appendix A of (d'Humières et al., 2002); (iii) RM model: Eq. (2.10) with $\omega_2 = 1.2 < \omega_1$ and f^{GE} given by Eq. (3.1). Note that the present choice of the second relaxation parameter $\omega_2 = 1.2$ is made in order to match the corresponding rate of the third-order moment relaxation of the MRT model of (d'Humières et al., 2002).

For the present RM model, the velocity vectors of the diagonally driven cavity flow for Re = 2000 at $z = 0.5$ (mid-plane parallel to the sliding plane) and the pressure field are reported in Fig. 1.

It has been already reported in (d'Humières et al., 2002) that the pressure field of the LBGK model in the present setup is severely contaminated by the checkerboard mode. Our simulation confirmed this observation. In Fig. 2, we report the velocity and the pressure fields as obtained by the MRT model of (d'Humières et al., 2002)
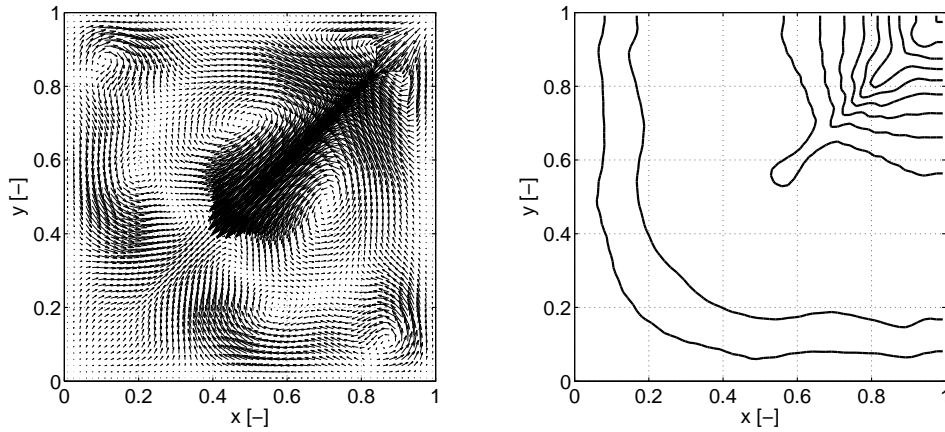
Figure 1. Present RM model. Left: Velocity vectors of the diagonally driven cavity flow for Re = 2000 at $z = 0.5$ (mid-plane); Right: Pressure contours. Numerical values of the pressure contour lines are -0.028:+0.002:-0.016.
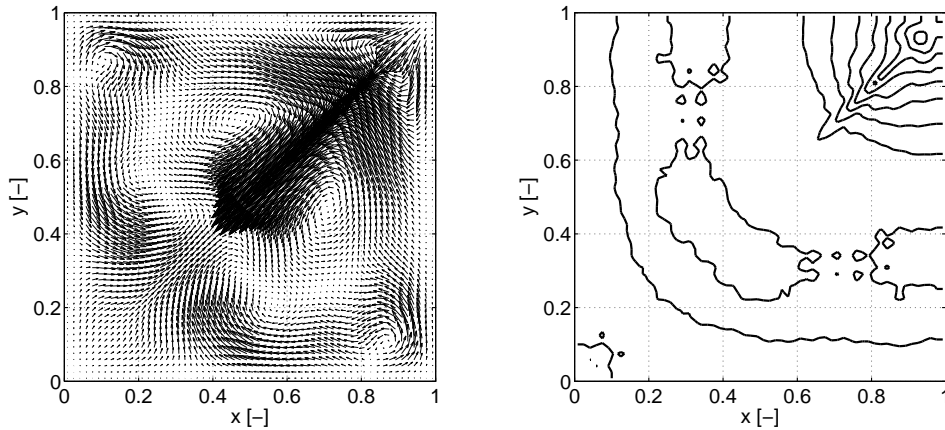

Figure 2. MRT model (d'Humières et al., 2002). Left: Velocity vectors; Right: Pressure contours (same values of pressure as in Fig. 1 shown). Parameters same as in Fig. 1. Numerical values of the pressure contour lines are -0.030:+0.002:-0.016.

(the realization of the MRT model as suggested in (d'Humières et al., 2002) was followed). Results presented in Fig. 2 are consistent with those of Ref. (d'Humières et al., 2002). Note that while the velocity fields are practically identical for the MRT and the present RM models, they both significantly improve the pressure, as compared to the LBGK case. Moreover, the present RM model does so essentially at a computational cost of the standard LBGK.

Summarizing, we have suggested a simple option for enhancing the stability and accuracy of the lattice Boltzmann models for incompressible flow simulations, by introducing a a two-step kinetic equation with a tailored intermediate relaxation state. The advantage of this revised matrix LB option is to considerably enlarging the stability domain of the most popular LBGK scheme, while retaining its simplic-

ity and computational efficiency. While the same idea also pertains to the matrix LB model, the present RM option is much simpler: instead of computing the whole set of moments at each grid node at each time step in order to execute the matrix LB collision, and to switch between the moment and the population representations from the collision to the propagation steps, in RM one needs to compute just a fraction of additional moments, while both the collision and propagation steps are executed in the populations space (as in the LBGK). Three dimensional simulations on the D3Q19 lattice indicate that the RM scheme enhances the LBGK model, basically at the same computational cost. The use of the two-step RM in this paper can be easily generalized to multi-step RM's with multiple intermediate states f^{C}. In general, the choice of intermediate states can be tailored to the enhancement of relaxation of various groups of moments. Remarkably, the implementation of RM is very straightforward, requiring, as it does, just the change of a few lines in existing LBGK codes. Based on the above, it is hoped that RM can be brought to broad fruition in lattice Boltzmann research at large.

References

C. K. Aidun and J. R. Clausen, Annu. Rev. Fluid. Mech. **42**, 439 (2010).

P. Asinari and I. Karlin, Physical Review E **79**, 36703 (2009).

P. Asinari and I. Karlin, Physical Review E **81**, 016702 (2010).

R. Benzi, S. Succi, and M. Vergassola, Phys. Rep. **222**, 145 (1992).

H. Chen, S. Chen, and W. Matthaeus, Phys. Rev. A **45**, R5339 (1992).

P. J. Dellar, Phys. Rev. E **64**, 031203 (2001).

A. N. Gorban and I. V. Karlin, Physica A **206**, 401 (1994).

D. d'Humières, in *Rarefied Gas Dynamics: Theory and Simulations (ed. B. D. Shizgal and D. P.Weaver)* (1992), vol. 159 of *AIAA Prog. Aeronaut. Astronaut.*, pp. 450–458.

D. d'Humières, I. Ginzburg, M. Krafczyk, P. Lallemand, and L.-S. Luo, Phil. Trans. R. Soc. Lond. A **360**, 437 (2002).

M. Geier, A. Greiner, and J. Korvink, Phys. Rev. E **73**, 066705 (2006).

I. Ginzburg, Adv. Water Resour. **28**, 1171 (2005).

F. Higuera, S. Succi, and R. Benzi, Europhys. Lett. **9**, 345 (1989).

I. V. Karlin, A. Ferrante, and H. C. Öttinger, Europhys. Lett. **47**, 182 (1999).

I. Karlin and P. Asinari, Physica A **389**, 1530 (2010).

Y.-H. Qian, D. d'Humieres, and P. Lallemand, Europhys. Lett. **17**, 479 (1992).

X. W. Shan and H. Chen, Int. J. Mod. Phys. C **18**, 635 (2007).